



Three-Dimensional Dirac Semimetal/Organic Thin Film Heterojunction Photodetector With Fast Response and High Detectivity

Qi Liu¹, Ming Yang¹, Jiangwei Zhang¹, Mingliang Yang¹, Jun Wang^{1,2}, Huajing Zheng^{1*} and Jun Gou^{1*}

¹ School of Optoelectronic Science and Engineering, University of Electronic Science and Technology of China, Chengdu, China, ² State Key Laboratory of Electronic Thin Films and Integrated Devices, University of Electronic Science and Technology of China, Chengdu, China

OPEN ACCESS

Edited by:

Xinping Zhang,
Beijing University of Technology, China

Reviewed by:

Zhen Wang,
Shanghai Institute of Technical
Physics (CAS), China
Man Luo,
Nantong University, China
Fu Xiao,
University of Chinese Academy of
Sciences, China

*Correspondence:

Huajing Zheng
zhj12@163.com
Jun Gou
goujun@uestc.edu.cn

Specialty section:

This article was submitted to
Optics and Photonics,
a section of the journal
Frontiers in Physics

Received: 26 February 2021

Accepted: 29 March 2021

Published: 23 April 2021

Citation:

Liu Q, Yang M, Zhang J, Yang M,
Wang J, Zheng H and Gou J (2021)
Three-Dimensional Dirac
Semimetal/Organic Thin Film
Heterojunction Photodetector With
Fast Response and High Detectivity.
Front. Phys. 9:672591.
doi: 10.3389/fphy.2021.672591

As a typical three-dimensional Dirac semimetal (3D DSM), Cd₃As₂ possess ultrahigh carrier mobility, high level of full spectral absorption, fast electron transmission speed, and high photocurrent response, which enable wide applications in infrared photodetector. However, the large dark current of the detector based on Cd₃As₂ thin film limits the application of the small current response. Hence, we demonstrated heterojunction photodetectors based on n-type 3D DSM Cd₃As₂ (pristine and Zn doped) and p-type organic (PbPc) by depositing PbPc thin film on Cd₃As₂ (pristine and Zn doped) thin film using thermal deposition method. These photodetectors can detect the radiation wavelength from 405 to 1,550 nm at room temperature. It is remarkable that this thin film heterojunction photodetector exhibits high detectivity (3.95×10^{11} Jones) and fast response time (160 μ s) under bias voltage, which is significantly improved vs. that of Cd₃As₂-based devices. The excellent performances are attributed to the strong built-in electric field at the interface of p-n junction, which is beneficial for efficient photocarriers collection and transportation. These results show that DSM/organic thin film heterojunction has excellent performance in the application of photodetectors. By combining 3D DSM with organic to form heterojunction, it provides a feasible solution for high-performance photodetectors.

Keywords: photodetector, Dirac semimetal, heterojunction, detectivity, response time

INTRODUCTION

Since the successful preparation of graphene in 2004 [1], graphene has been widely studied due to its excellent carrier transport performance, unique two-dimensional (2D) energy dispersion, and stable electrical and optical properties [2–4]. At present, graphene has shown extremely high application value in many fields such as photoelectric detection, solar cell and optical modulator [5–11]. However, due to the limitations of the natural ultrathin structure of 2D materials, graphene inevitably has shortcomings such as vulnerable to external dielectric interference, weak absorbance and lack of controllable physical space [12–14]. Recently, “three-dimensional (3D) graphene”—3D Dirac semimetal (DSM), a quantum topology material, has attracted much attention. As 3D graphene, Cd₃As₂ has electronic band structure with zero band gap and linear energy

dispersion [15–18]. And Cd_3As_2 has extremely high carrier mobility, which can reach $9 \times 10^6 \text{ cm}^2/(\text{Vs})$ (below 5 K) [19]. Moreover, compared with graphene, the electronic properties of Cd_3As_2 are better protected to prevent surface and environment change [20]. Owing to all these characteristics above mentioned, the 3D DSM provides an excellent platform for the fabrication of high-performance photodetectors.

With the gradually mature development of growing Cd_3As_2 technology, varieties of photodetectors based on Cd_3As_2 thin film or nanocrystal have been prepared and reported. Wang et al. reported the realization of a broadband photodetector based on Cd_3As_2 nanoplate and nanowire, which exhibits broadband detection capability (from 532 to $10.6 \mu\text{m}$) and had a maximum responsivity (R_i) of 5.9 mA/W [21]. Yavarishad et al. demonstrated an infrared photodetector based on Cd_3As_2 crystals. The maximum R_i of the photodetector is 0.27 mA/W [22]. Meng et al. experimentally proved the saturated absorption effect of Cd_3As_2 thin film across 1–2 μm [23]. However, due to semimetal properties of Cd_3As_2 , results in a large dark current of devices. One possible solution to the above predicament is to design a p-n heterojunction photodetector [24]. For example, Yang et al. demonstrated a wideband photodetector based on heterojunction of Cd_3As_2 thin film and pentacene, which can detect the radiation wavelength from 450 to $10.6 \mu\text{m}$ with a maximum R_i of 36.15 mA/W at room temperature [25]. After that, Yang et al. continued to prepared heterojunction devices which were fabricated by Cd_3As_2 thin film with organics (small molecules and polymers), whose detection range was from 450 to $10.6 \mu\text{m}$ with a maximum R_i of 729 mA/W [26]. On the other hand, in order to reduce the electron density and open the band gap, Zn doping is used to compensate for the residual electron concentration of Cd_3As_2 [27, 28]. Yang et al. reported photodetectors based on $(\text{Cd}_{1-x}\text{Zn}_x)_3\text{As}_2/\text{MoO}_3$ heterojunction [29], showing ultrahigh R_i and detectivity (D^*) of 3.1 A/W and 6.4×10^{10} Jones, respectively.

Compared with the inorganic, organic are more promising for the combination with Cd_3As_2 thin film because of easy large area and low-cost fabrication. Lead phthalocyanine (PbPc) is a kind of hole transport material, but its hole mobility is only about 10^{-6} – $10^{-4} \text{ cm}^2/(\text{Vs})$ [30]. Moreover, PbPc is selected as the p-type material in heterojunction photodetectors because it is a good candidate for near-infrared absorbing material [31–33]. In this article, we prepared wide-band photodetector with a heterojunction structure, which were fabricated by Cd_3As_2 and $(\text{Cd}_{1-x}\text{Zn}_x)_3\text{As}_2$ thin film with the PbPc. Therefore, we designed and utilized the chemical doping and p-n heterojunction structure, which greatly improve the photoelectric performance of Cd_3As_2 thin film devices. The DSM/organic thin film heterojunction devices exhibit excellent photocurrent response and very small dark current. Moreover, these devices have higher D^* (the maximum D^* can reach 3.95×10^{11} Jones) and faster response time (160/170 μs) than those of previously reported photodetectors based on the Cd_3As_2 thin film. Use of DSM thin film and organic molecules also opens up a new path for the practical application of DSM materials.

EXPERIMENTAL SECTION

Devices Preparation

Cd_3As_2 and $(\text{Cd}_{1-x}\text{Zn}_x)_3\text{As}_2$ thin films were produced by molecular-beam epitaxy (MBE) system when the vacuum lower than 2×10^{-8} Pa, PbPc thin film and Au electrodes were prepared by thermal deposition when the vacuum lower than 6×10^{-4} Pa. Before growing the DSM layer, the substrates were degassed at 400°C for 30 min to remove gas molecules adsorbed on the surface. Then, the CdTe buffer layer began to grow in order to achieve a better crystalline match. The DSM thin films deposition was carried out on the top of the buffer layer. The substrate with 100 nm DSM thin films was placed into the evaporation equipment to deposit 100 nm PbPc thin film. The electrodes is also prepared by the thermal evaporation method, and the thickness of the electrodes is 60 nm. Finally, the photodetectors of DSM/PbPc thin film were fabricated with a channel of $200 \times 200 \mu\text{m}$.

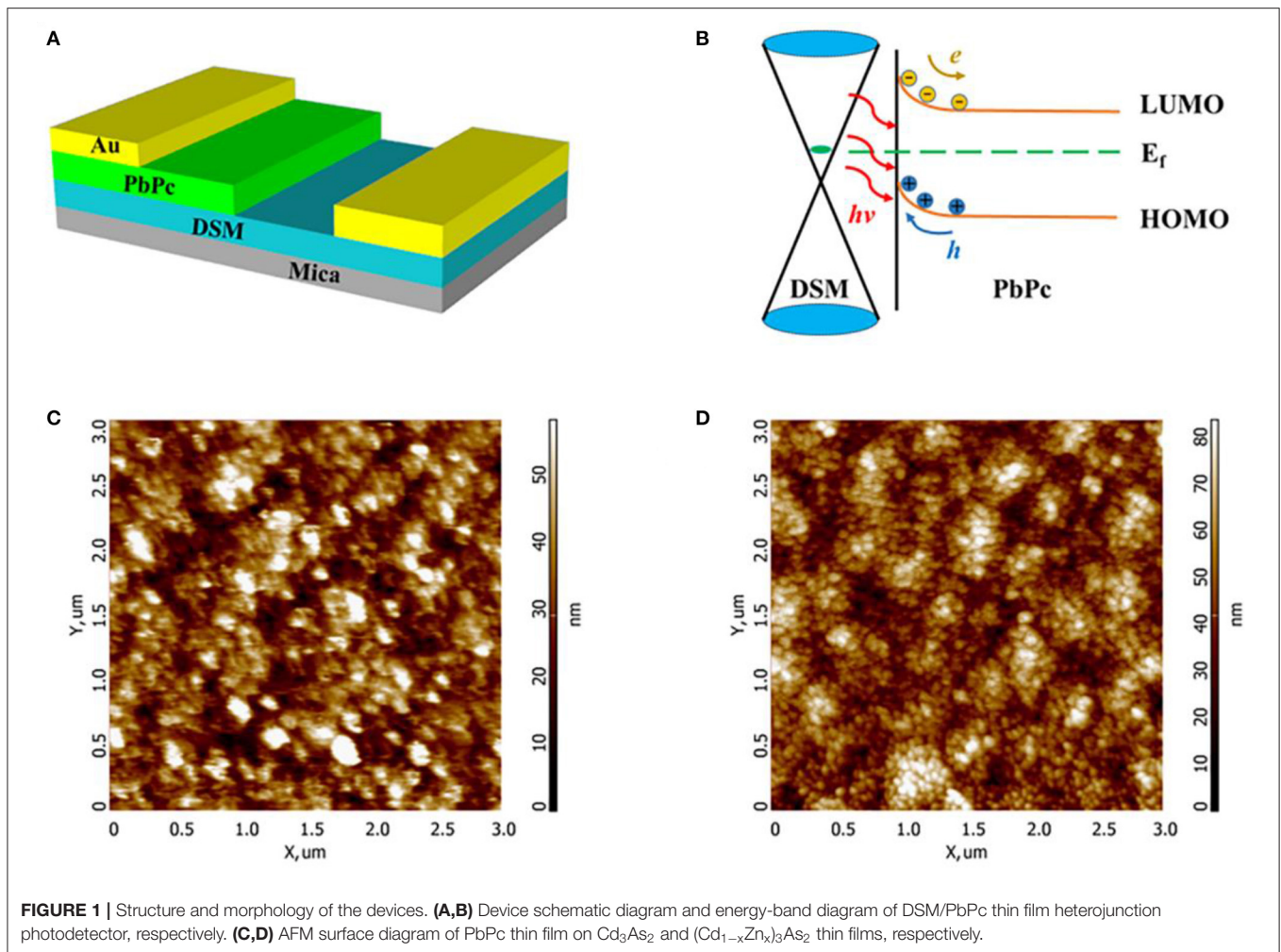
Characterization

The surface morphology of thin film was studied by atomic force microscopy (AFM). The photoelectric performances were measured by the Keithley 2636B source meter system and FS-Pro all-in-one multifunctional semiconductor parameter testing system. The laser power was measured by Ophir RM9 system, and the measurement range is 100 to 100 mW.

RESULTS AND DISCUSSION

We directly prepare electrodes on the DSM thin films by thermal evaporation, **Supplementary Figure 1** shows the schematic of DSM thin film device. From the **Supplementary Figure 2**, we can find that the dark current of $(\text{Cd}_{1-x}\text{Zn}_x)_3\text{As}_2$ thin film is ~ 10 times smaller than that of pristine Cd_3As_2 . Meanwhile, the photocurrent of $(\text{Cd}_{1-x}\text{Zn}_x)_3\text{As}_2$ thin film is slightly smaller than that of Cd_3As_2 thin film. This result is mainly due to the doping of Zn ion, which reduces the conductivity of the thin film, but the response to light changes little.

Next, we prepared heterojunction photodetectors based on DSM and p-type organic. The structure of the vertical heterojunction devices is shown in **Figure 1A**, from top to bottom, the layers are Au, PbPc, DSM, and mica. Once the DSM thin film is in contact with the PbPc thin film, due to the difference in Fermi level between them, electrons flow from the n-type Cd_3As_2 into the lower energy states in p-type PbPc, forming a negative space charge region on the semiconductor surface. At this time, there is a certain electric field in the space charge region, which causes the energy band bend upward (**Figure 1B**). When the device is illuminated by light, photogenerated electrons/holes are generated at the interface between DSM and organic. Then they separate in the junction region and transport to the two electrodes, respectively, because of the built-in electric field. **Figures 1C,D** demonstrate surface topography of PbPc thin film on DSM thin films. The root-mean-square (RMS) roughness of PbPc thin film on Cd_3As_2 and $(\text{Cd}_{1-x}\text{Zn}_x)_3\text{As}_2$ thin films are 12.83 and 14.27 nm, respectively.



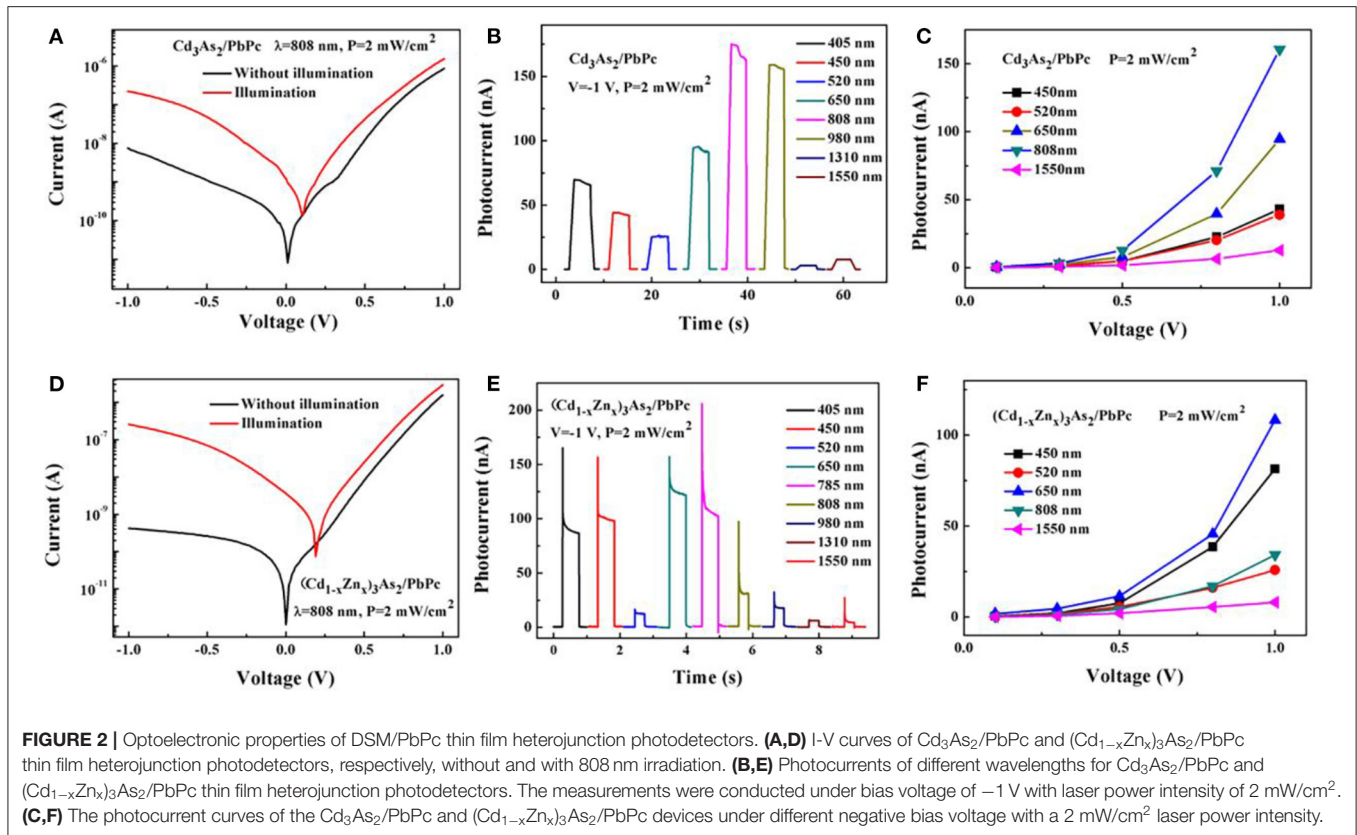
It can be clearly seen that the films made of the two materials are uniform and dense. Therefore, the film quality of the two composite thin films is very good, which can meet the needs of fabricating devices.

Figure 2 shows the optoelectronic properties of DSM/PbPc thin film heterojunction devices. The I-V curves of $\text{Cd}_3\text{As}_2/\text{PbPc}$ and $(\text{Cd}_{1-x}\text{Zn}_x)_3\text{As}_2/\text{PbPc}$ devices are shown in **Figures 2A,D**. The dark current of the device is small under the reverse bias voltage, while the dark current increases exponentially with the voltage under the forward bias voltage, which is consistent with the I-V curve of the typical photodiode, and has significant rectification characteristics. The rectification ratio at $\pm 1\text{ V}$ is close to 10^3 , indicating that a heterojunction is formed between the Cd_3As_2 thin film and the organic thin film. Compared with the $\text{Cd}_3\text{As}_2/\text{PbPc}$ device, the dark current and the photocurrent of $(\text{Cd}_{1-x}\text{Zn}_x)_3\text{As}_2/\text{PbPc}$ photodetector are decreased from 7.5 to 0.42 nA, and 223 to 124 nA, when illuminated under 808 nm laser source whose laser power intensity is 2 mW/cm^2 with $V_{\text{bias}} = -1\text{ V}$. The on-off ratio of $(\text{Cd}_{1-x}\text{Zn}_x)_3\text{As}_2/\text{PbPc}$ photodetector is as high as 295 under the bias voltage of -1 V , almost 10 times that of $\text{Cd}_3\text{As}_2/\text{PbPc}$

photodetector 29.7. The result show that heterojunction can significantly reduce the dark current of Cd_3As_2 thin film devices, and the effect of doped Cd_3As_2 devices is more obvious. In order to find the best bias voltage for the best test effect, these photodetectors use $V_{\text{bias}} = -1\text{ V}$ as the main test bias voltage.

When the DSM/PbPc devices are biased at -1 V , the photocurrent response of different wavelength bands (from 405 to 1,550 nm) is shown in **Figures 2B,E**. We can clearly see that the device has good photocurrent response from visible light to near-infrared region. As the wavelength gradually rises, the photocurrent falls first and then rises, which is related to the absorption spectrum of PbPc (**Supplementary Figure 3**). In addition, as shown in **Figures 2C,F**, the photodetectors can produce a much stronger photocurrent when it works under the bias voltage mode.

R_i is used to characterize the excellent performance of optoelectronic device. In general, R_i is the ability of the photodetector to convert optical signal into electrical signal, which is defined as the ratio of the photocurrent detected by the device to the power of the incident light source. D^* is



an important index to measure the limit detection ability of photodetectors for weak signals. The formulas are as follows:

$$R_i = \frac{I_{ph}}{P} = \frac{I_L - I_D}{P} \quad (1)$$

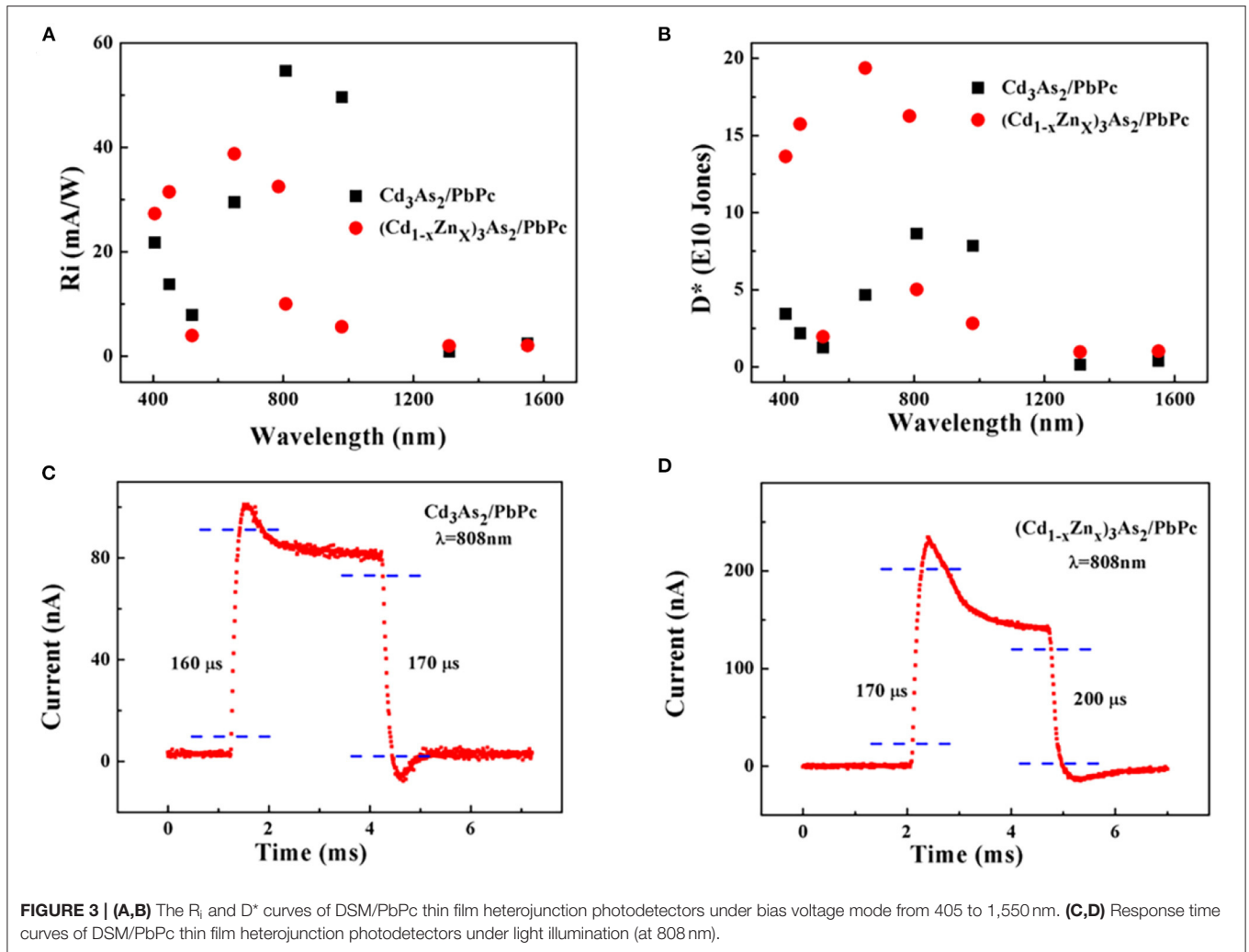
$$D^* = \frac{R_i \sqrt{S}}{\sqrt{2qI_D}} \quad (2)$$

Among them, I_{ph} is photogenerated current on the active channel area, I_L is current under the illumination, I_D is dark current (without illumination), and P is laser power. Moreover, S and q , respectively, represent the active area and the charge per electron [34–36].

Figure 3A is the R_i diagram of the DSM/PbPc devices. The measurements were conducted under bias voltage of -1 V with laser power intensity of 2 mW/cm². The maximum R_i of Cd₃As₂/PbPc device at 808 nm is 54.6 mA/W. The (Cd_{1-x}Zn_x)₃As₂/PbPc device has a maximum R_i of 38.8 mA/W at 650 nm. **Figure 3B** is the D^* calculated based on the measured experimental data. The maximum D^* of Cd₃As₂/PbPc is 8.62×10^{10} Jones at 808 nm. The maximum D^* of (Cd_{1-x}Zn_x)₃As₂/PbPc device at 650 nm is 1.93×10^{11} Jones, which is the maximum value obtained in the devices based on Cd₃As₂. The high D^* can be attributed to be the lower dark current at reverse bias voltage. The EQE curve is shown in

Supplementary Figure 4. Accordingly, the largest values are 8.4 and 8.6%, respectively.

Moreover, the response time has traditionally been considered to be a significant feature of photodetector [37, 38]. **Figures 3C,D** is the response time curves of the device. The response time of Cd₃As₂/PbPc device is 160/170 μs, and that of (Cd_{1-x}Zn_x)₃As₂/PbPc device is 170/200 μs. It can be observed in the figure that there is an obvious “peak” in the rising process, which is usually related to the charge trapping effect existing in the carrier transport process inside the device [35, 39, 40]. Specifically, at the moment when light begins to irradiate the device, the photogenerated exciton at the interface of the device are dissociated into holes and electrons under the action of the built-in electric field, and then rapidly transport to the two electrodes, respectively. If there is charge trapping traps in a certain interface or layer, some of the free carriers will be filled with these traps. With the filling of the traps, the original built-in electric field is gradually weakened, resulting in the decrease of the number of carriers collected by the two electrodes in unit time, so the photocurrent gradually decreases. Until the recombination of carrier transmission and trap induction achieves a dynamic balance, the photocurrent can achieve a steady state, so the “peak” phenomenon can be seen in the rising part of the transient photocurrent [41, 42]. At the same time, there is a reverse “peak” in the falling process, which reflects the phenomenon that the interface charge cannot be effectively

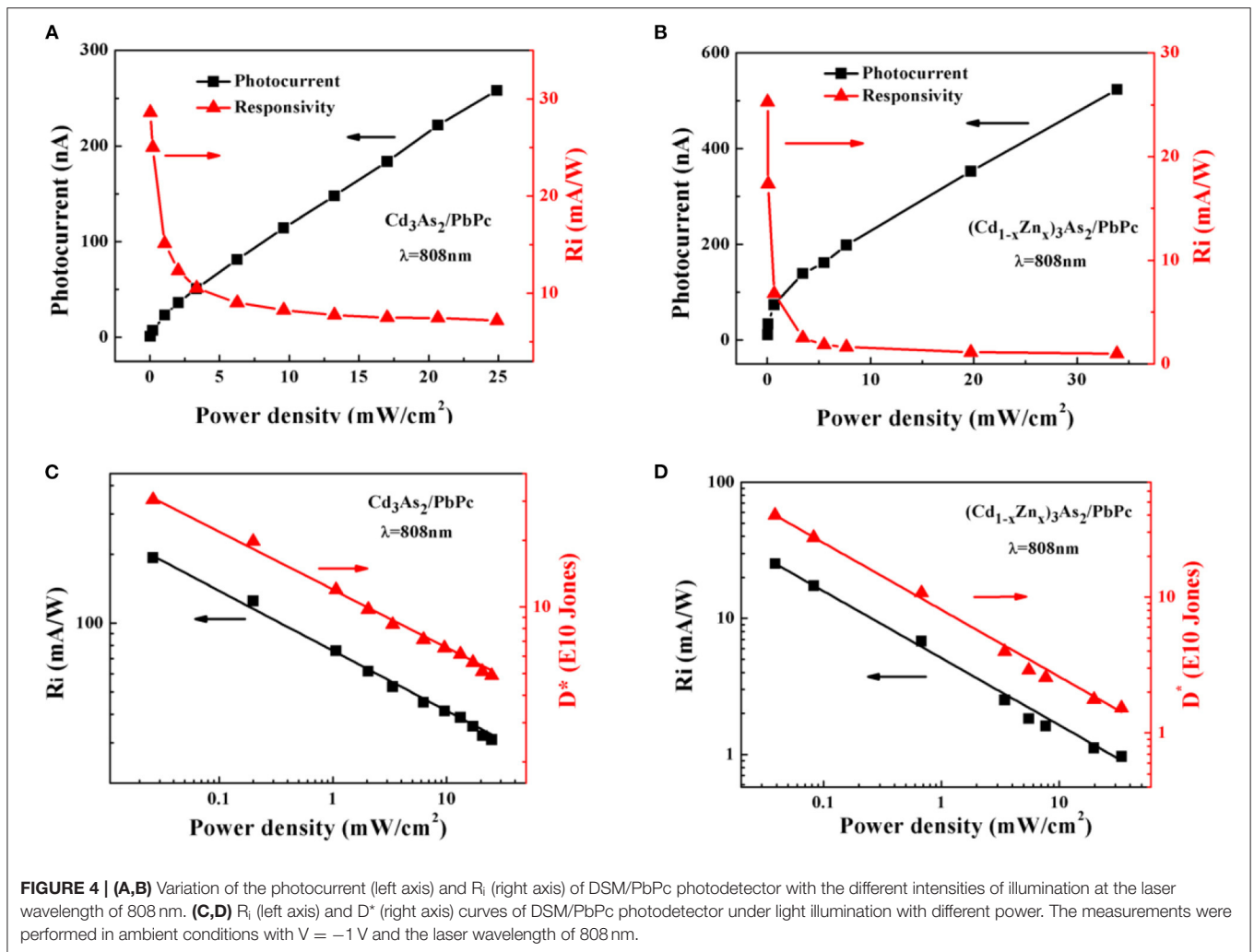


extracted when the light is stopped suddenly [43]. Moreover, the peak may also be related to the charge and discharge of the heterojunction capacitor.

We further investigated the incident light power dependence of the photoresponse in both the DSM/PbPc thin film heterojunction photodetector, and the major results are plotted in **Figure 4**, respectively (measured at $V = -1$ V in ambient conditions). The relationship among R_i , photocurrent and incident laser power is shown in **Figures 4A,B**. With the increase of optical power, the photocurrent of the device also increases, and the photocurrent tends to be saturated at higher optical power. This non-linear relationship is the final result of a series of complex processes, including the generation of photogenerated carriers in near the DSM/PbPc interface, the photogenerated carriers transport through the interface, and the photogenerated carriers are trapped and compounded by defects [44]. Also, with the increase of incident power, the R_i is inversely proportional to the incident power, and the higher R_i often occurs when the power is relatively low. Due to most of the defect states are not occupied at low power,

and the holes generated after illumination are captured, so the R_i is high. With the increase of the incident light power, the captured states are occupied and tend to be saturated, and the built-in electric field decreases, and the R_i gradually decreases due to this effect. As shown in **Figures 4C,D**, the calculated R_i and D^* under illumination of 808 nm with various light intensity are obtained, respectively, at room temperature. We can see the R_i and D^* of two photodetector decreases with the power increasing. The R_i and D^* of $\text{Cd}_3\text{As}_2/\text{PbPc}$ reach up to 193 mA/W and 3.05×10^{11} Jones at $0.03 \text{ mW}/\text{cm}^2$, respectively. And, the R_i and D^* of $(\text{Cd}_{1-x}\text{Zn}_x)_3\text{As}_2/\text{PbPc}$ reach up to 25 mA/W and 3.95×10^{11} Jones at $0.03 \text{ mW}/\text{cm}^2$, respectively.

To understand the above-mentioned excellent ultra-high D^* and high response speed performance of device, the mechanisms are proposed here to elucidate this in detail. The response speed of photodetector is determined by the separation and transport speed of the photogenerated charge carriers. For our photodetector based on p-n heterojunction, there are three main reasons for the fast response speed: (1) The vertical



heterojunction structure has intrinsically short transport length for carriers [45]. (2) The strong built-in electric field from the DSM and PbPc thin film can greatly facilitate the separation and collection of the photocarriers, inducing the high response speed [46, 47]. (3) Moreover, when the heterojunction is applied with reverse bias voltage, the electric field caused by reverse bias is consistent with the built-in electric field, so the barrier height is enhanced. Meanwhile, the photogenerated minority carriers can pass through the interface easier owing to the strong external electric field [48]. All of the features work synergistically for fast transport of photogenerated charge carriers at the respective electrodes. In addition, the high D^* can be attributed to be the excellent diode behavior with a lower dark current at reverse bias voltage. Moreover, the low reverse dark current thus is conducive to enhance low light detection capability of the photodetector.

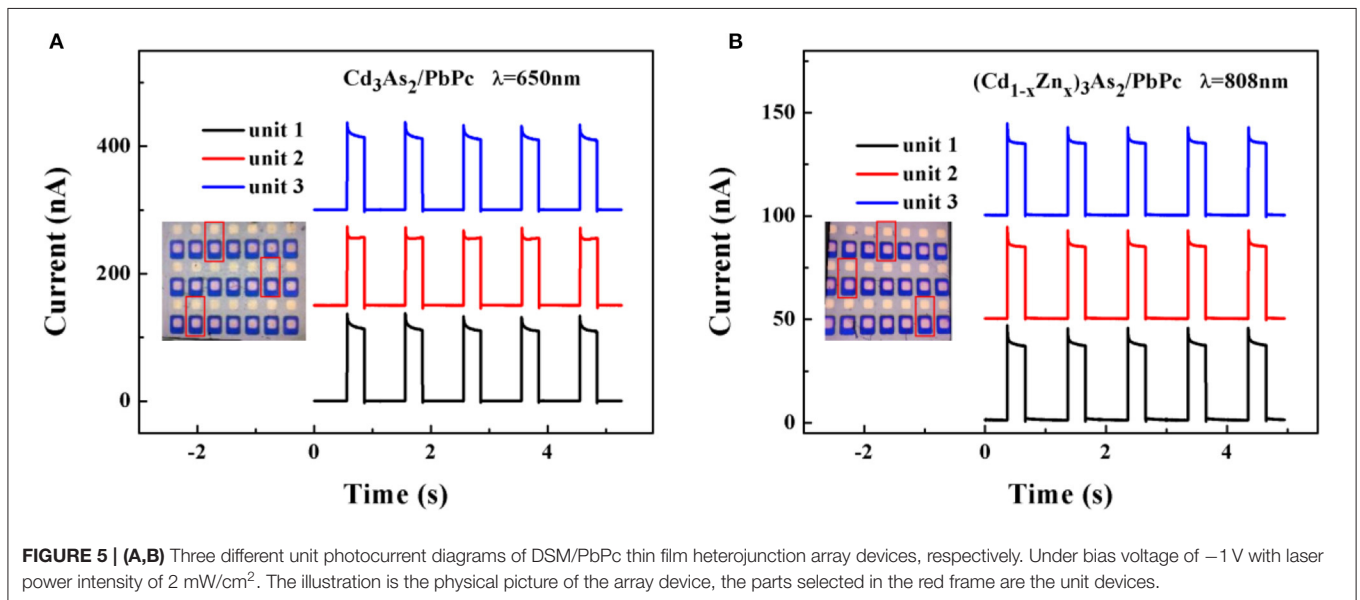
Comparison of the performance of DSM/PbPc heterojunction photodetector with Cd_3As_2 based devices in the literature, some key parameters of the photodetector are summarized in **Table 1**. It is noted that the heterojunction devices fabricated by us

have a relatively high D^* and a fast response speed with light intensity of 2 mW/cm^2 compared with the reported Cd_3As_2 based photodetectors. However, the excellent performance of the devices on the fast response speed was achieved by sacrificing R_i , the DSM/PbPc heterojunction devices fabricated by us have a relatively low R_i compared with the others. Especially, compared with the $(\text{Cd}_{1-x}\text{Zn}_x)_3\text{As}_2/\text{MoO}_3$ heterojunction device. These excellent performances of the p-n heterojunction photodetector indicate that this device may have great potential applications in the low light signals photodetection.

The unit stability of array device is an important performance index of array devices. In this work, we stochastically tested three different units in the DSM/PbPc thin film heterojunction array devices, respectively, as shown in **Figures 5A,B**. We found that the current properties of different units in each array device were basically consistent, and the units has good stability and repeatability. This result shows the potential of DSM thin film in the fields of array applications.

TABLE 1 | Performance of photodetectors based on Cd_3As_2 material.

No.	Active materials	R_i (mA/W)	Wavelength range (nm)	$\tau_{\text{on}}/\tau_{\text{off}}$ (ms)	D^* (Jones)	References
1	Cd_3As_2 crystal nanowire/plate	5.9	532–10,600	6.9ps	/	[19]
2	Cd_3As_2 crystal platelets	0.27	1,064	/	/	[20]
3	Cd_3As_2 /pentacene thin film	36.15	450–10,600	44/124	1.9×10^7	[22]
4	Cd_3As_2 /DPEPO	729	365–10,600	16.32/23.75	7.9×10^9	[23]
5	Cd_3As_2 /PEDOT:PSS	81.3	365–10,600	1.87/1.94	1.1×10^9	[23]
6	$(\text{Cd}_{1-x}\text{Zn}_x)_3\text{As}_2/\text{MoO}_3$	3,100	405–4,500	30/280	6.4×10^{10}	[30]
7	$\text{Cd}_3\text{As}_2/\text{PbPc}$	193	405–1,550	0.16/0.17	3.05×10^{11}	This work
8	$(\text{Cd}_{1-x}\text{Zn}_x)_3\text{As}_2/\text{PbPc}$	38.8	405–1,550	0.17/0.2	3.95×10^{11}	This work



CONCLUSION

In conclusion, we have successfully fabricated 3D DSM/organic thin film heterojunction photodetectors. These devices have good R_i , up to 193 mA/W (at 808 nm of $\text{Cd}_3\text{As}_2/\text{PbPc}$), and excellent D^* of 3.95×10^{11} Jones [at 808 nm of $(\text{Cd}_{1-x}\text{Zn}_x)_3\text{As}_2/\text{PbPc}$], which is the maximum value measured in all Cd_3As_2 based thin film devices. Meantime, the device in this work has faster $\tau_{\text{on}}/\tau_{\text{off}}$ (160/170 μs and 170/200 μs for $\text{Cd}_3\text{As}_2/\text{PbPc}$ heterojunction and $(\text{Cd}_{1-x}\text{Zn}_x)_3\text{As}_2/\text{PbPc}$ heterojunction) than the previous Cd_3As_2 based devices. In this paper, the DSM and organic heterojunction photodetectors have the advantages of simple structure, easy preparation and low cost, which are suitable for industrial promotion. Moreover, the development direction of array is also studied, which can adapt to the future market demand for high-performance photodetectors.

DATA AVAILABILITY STATEMENT

The original contributions presented in the study are included in the article/**Supplementary Material**, further inquiries can be directed to the corresponding author/s.

AUTHOR CONTRIBUTIONS

JW designed and conducted this work. QL and MY conducted experimental measurement and data analysis. JZ, MY, HZ, and JG provided suggestions and assistance to this experiment. All authors discussed the experimental results.

FUNDING

This work was supported by National Outstanding Youth Science Fund Project of National Natural Science Foundation of China (No. 61922022), Science Fund for Innovative Research Group Project of the National Natural Science Foundation of China (No. 61421002), the Sichuan Science and Technology Program (Grant No. 2020JDR0061).

SUPPLEMENTARY MATERIAL

The Supplementary Material for this article can be found online at: <https://www.frontiersin.org/articles/10.3389/fphy.2021.672591/full#supplementary-material>

REFERENCES

- Novoselov KS, Geim AK, Morozov SV, Jiang D, Zhang Y, Dubonos SV, et al. Electric field effect in atomically thin carbon films. *Science*. (2004) 306:666–9. doi: 10.1126/science.1102896
- Chen K, Yogeesh MN, Huang Y, Zhang SQ, He F, Meng XH, et al. Non-destructive measurement of photoexcited carrier transport in graphene with ultrafast grating imaging technique. *Carbon*. (2016) 107:233–9. doi: 10.1016/j.carbon.2016.05.075
- Wang JG, Mu XJ, Sun MT. The thermal, electrical and thermoelectric properties of graphene nanomaterials. *Nanomaterials*. (2019) 9:218. doi: 10.3390/nano9020218
- Zhang SJ, Li ZW, Xing F. Review of polarization optical devices based on graphene materials. *Int J Mol Sci*. (2020) 21:1608. doi: 10.3390/ijms21051608
- Han JY, Wang J, Yang M, Kong X, Chen XQ, Huang ZH, et al. Graphene/organic semiconductor heterojunction phototransistors with broadband and bi-directional photoresponse. *Adv Mater*. (2018) 30:1804020. doi: 10.1002/adma.201804020
- Ni ZY, Ma LL, Du SC, Xu Y, Yuan M, Fang HH, et al. Plasmonic silicon quantum dots enabled high-sensitivity ultrabroadband photodetection of graphene-based hybrid phototransistors. *ACS Nano*. (2017) 11:9854–62. doi: 10.1021/acsnano.7b03569
- Ishikawa R, Yamazaki S, Watanabe S, Tsuboi N. Layer dependency of graphene layers in perovskite/graphene solar cells. *Carbon*. (2021) 172:597–601. doi: 10.1016/j.carbon.2020.10.065
- Khan U, Kim TH, Ryu H, Seung W, Kim SW. Graphene tribotronics for electronic skin and touch screen applications. *Adv Mater*. (2017) 29:1603544. doi: 10.1002/adma.201603544
- Luo SY, Wang YN, Tong X, Wang ZM. Graphene-based optical modulators. *Nanoscale Res Lett*. (2015) 10:1–11. doi: 10.1186/s11671-015-0866-7
- Hu X, Wang J. Design of graphene-based polarization-insensitive optical modulator. *Nanophotonics*. (2018) 7:651–8. doi: 10.1515/nanoph-2017-0088
- Han J, He M, Yang M, Han Q, Wang F, Zhong F, et al. Light-modulated vertical heterojunction phototransistors with distinct logical photocurrents. *Light-Sci App*. (2020) 9:167. doi: 10.1038/s41377-020-00406-4
- Sidorov AN, Slawinski GW, Jayatissa AH, Zamborini FP, Sumanasekera GU. A surface-enhanced Raman spectroscopy study of thin graphene sheets functionalized with gold and silver nanostructures by seed-mediated growth. *Carbon*. (2012) 50:699–705. doi: 10.1016/j.carbon.2011.09.030
- Lin YC, Lu CC, Yeh CH, Jin CH, Suenaga K, Chiu PW. Graphene annealing: how clean can it be? *Nano Lett*. (2012) 12:414–9. doi: 10.1021/nl203733r
- Wang HD, Zhang X, Takamatsu H. Ultraclean suspended monolayer graphene achieved by *in situ* current annealing. *Nanotechnology*. (2017) 28:045706. doi: 10.1088/1361-6528/28/4/045706
- Krizman G, Schumann T, Tchoumakov S, Assaf BA, Stemmer S, de Vaulchier LA, et al. Determination of the crystal field splitting energy in Cd₃As₂ using magnetooptics. *Phys Rev B*. (2019) 100:155205. doi: 10.1103/PhysRevB.100.155205
- Chorsi HT, Yue SY, Iyer PP, Goyal M, Schumann T, Stemmer S, et al. Widely tunable optical and thermal properties of dirac semimetal Cd₃As₂. *Adv Opt Mater*. (2020) 8:1901192. doi: 10.1002/adom.201901192
- Yang YK, Xiu FX, Wang FQ, Wang J, Shi Y. Electrical transport and optical properties of Cd₃As₂ thin films. *Chin Phys B*. (2019) 28:107502. doi: 10.1088/1674-1056/ab3a91
- Roth S, Lee H, Sterzi A, Zacchigna M, Politano A, Sankar R, et al. Reinvestigating the surface and bulk electronic properties of Cd₃As₂. *Phys Rev B*. (2018) 97:165439. doi: 10.1103/PhysRevB.97.165439
- Liang T, Gibson Q, Ali MN, Liu MH, Cava RJ, Ong NP. Ultrahigh mobility and giant magnetoresistance in the Dirac semimetal Cd₃As₂. *Nat Mater*. (2015) 14:280–4. doi: 10.1038/nmat4143
- Liu ZK, Jiang J, Zhou B, Wang ZJ, Zhang Y, Weng HM, et al. A stable three-dimensional topological Dirac semimetal Cd₃As₂. *Nat Mater*. (2014) 13:677–81. doi: 10.1038/nmat3990
- Wang QS, Li CZ, Ge SF, Li JG, Lu W, Lai JW, et al. Ultrafast Broadband Photodetectors Based on Three-Dimensional Dirac Semimetal Cd₃As₂. *Nano Lett*. (2017) 17:834–41. doi: 10.1021/acs.nanolett.6b04084
- Yavarishad N, Hosseini T, Kheirandish E, Weber CP, Kouklin N. Room-temperature self-powered energy photodetector based on optically induced Seebeck effect in Cd₃As₂. *Applied Physics Express*. (2017) 10(5). doi: 10.7567/APEX.10.052201
- Meng YF, Zhu CH, Li Y, Yuan X, Xiu FX, Shi Y, et al. Three-dimensional Dirac semimetal thin-film absorber for broadband pulse generation in the near-infrared. *Opt Lett*. (2018) 43:1503–6. doi: 10.1364/OL.43.001503
- Han JY, Wang J. Photodetectors based on two-dimensional materials and organic thin-film heterojunctions. *Chin Phys B*. (2019) 28:017103. doi: 10.1088/1674-1056/28/1/017103
- Yang M, Wang J, Han JY, Ling JW, Ji CH, Kong X, et al. Enhanced performance of wideband room temperature photodetector based on Cd₃As₂ thin film/pentacene heterojunction. *ACS Photonics*. (2018) 5:3438–45. doi: 10.1021/acsp Photonics.8b00727
- Yang M, Wang J, Yang YK, Zhang Q, Ji CH, Wu GR, et al. Ultraviolet to long-wave infrared photodetectors based on a three-dimensional dirac semimetal/organic thin film heterojunction. *J Phys Chem Lett*. (2019) 10:3914–21. doi: 10.1021/acs.jpcllett.9b01619
- Lu H, Zhang X, Bian Y, Jia S. Topological phase transition in single crystals of (Cd_{1-x}Znx)₃As₂. *Sci Rep*. (2017) 7:3148. doi: 10.1038/s41598-017-03559-2
- Nishihaya S, Uchida M, Nakazawa Y, Akiba K, Kriener M, Kozuka Y, et al. Negative magnetoresistance suppressed through a topological phase transition in (Cd_{1-x}Znx)₃As₂ thin films. *Phys Rev B*. (2018) 97:245103. doi: 10.1103/PhysRevB.97.245103
- Yang M, Yang Y, Liu Q, Zhou H, Han J, Xie X, et al. A 3D topological Dirac semimetal/MoO₃ thin film heterojunction infrared photodetector with a current reversal phenomenon. *J Mater Chem C*. (2020) 8:16024–31. doi: 10.1039/D0TC03374J
- Su ZS, Hou FH, Wang X, Gao Y, Jin FM, Zhang G, et al. High-performance organic small-molecule panchromatic photodetectors. *ACS Appl Mater Interfaces*. (2015) 7:2529–34. doi: 10.1021/am5074479
- Choi MS, Lee S, Kim HJ, Kim JJ. Inverted near-infrared organic photodetector with oriented lead (II) phthalocyanine molecules via substrate heating. *Org Electron*. (2018) 61:164–9. doi: 10.1016/j.orgel.2018.05.038
- Wu L, Xu R, Yao G, Su D, Su Z, Yang H. Photomultiplication type near-infrared organic photodetectors with a mixed active layer. *Microwave Optical Technol Lett*. (2021) 63:714–8. doi: 10.1002/mop.32647
- Mukherjee B, Mukherjee M. Programmable memory in organic field-effect transistor based on lead phthalocyanine. *Org Electron*. (2009) 10:1282–7. doi: 10.1016/j.orgel.2009.07.006
- Fu W, Ma H, Wei Y, Jiang KL, Fei GT, Zhang LD. Preparation and infrared response properties of vanadium dioxide nanowire/carbon nanotube composite film. *J Mater Sci*. (2017) 52:7224–31. doi: 10.1007/s10853-017-0959-z
- Miao JS, Song B, Li Q, Cai L, Zhang SM, Hu WD, et al. Photothermal effect induced negative photoconductivity and high responsivity in flexible black phosphorus transistors. *ACS Nano*. (2017) 11:6048–56. doi: 10.1021/acsnano.7b01999
- Zhu MS, Huang Y, Huang Y, Li HF, Wang ZF, Pei ZX, et al. A highly durable, transferable, and substrate-versatile high-performance all-polymer micro-supercapacitor with plug-and-play function. *Adv Mater*. (2017) 29:605137. doi: 10.1002/adma.201605137
- Zhong HJ, Xu K, Liu ZH, Xu GZ, Shi L, Fan YM, et al. Charge transport mechanisms of graphene/semiconductor Schottky barriers: a theoretical and experimental study. *J Appl Phys*. (2014) 115:59500. doi: 10.1063/1.4859500
- Zhang KA, Zhang TN, Cheng GH, Li TX, Wang SX, Wei W, et al. Interlayer transition and infrared photodetection in atomically thin Type-II MoTe₂/MoS₂ van der Waals heterostructures. *ACS Nano*. (2016) 10:3852–8. doi: 10.1021/acsnano.6b00980
- Hwang I, McNeill CR, Greenham NC. Drift-diffusion modeling of photocurrent transients in bulk heterojunction solar cells. *J Appl Phys*. (2009) 106:47547. doi: 10.1063/1.3247547
- Li Z, Gao F, Greenham NC, McNeill CR. Comparison of the operation of polymer/fullerene, polymer/polymer, and polymer/nanocrystal solar cells: a transient photocurrent and photovoltage study. *Adv Funct Mater*. (2011) 21:1419–31. doi: 10.1002/adfm.201002154
- Tress W, Corvers S, Leo K, Riede M. Investigation of driving forces for charge extraction in organic solar cells: transient photocurrent measurements on solar cells showing S-shaped current-voltage characteristics. *Adv Energy Mater*. (2013) 3:873–80. doi: 10.1002/aenm.201200931

42. Fang Y, Hou Y, Hu Y, Teng F. Transient photocurrent response of plasmon-enhanced polymer solar cells with gold nanoparticles. *Materials*. (2015) 8:4050–60. doi: 10.3390/ma8074050
43. Wang TN, Wang Y, Zhu LJ, Lv LF, Hu YF, Deng ZB, et al. High sensitivity and fast response sol-gel ZnO electrode buffer layer based organic photodetectors with large linear dynamic range at low operating voltage. *Org Electron*. (2018) 56:51–8. doi: 10.1016/j.orgel.2018.08.017
44. Huang ZH, Jiang YD, Han Q, Yang M, Han JY, Wang F, et al. High responsivity and fast UV-vis-short-wavelength IR photodetector based on Cd₃As₂/MoS₂ heterojunction. *Nanotechnology*. (2020) 31:064001. doi: 10.1088/1361-6528/ab51d3
45. Yang M, Wang J, Zhao YF, He L, Ji CH, Liu XC, et al. Three-dimensional topological insulator Bi₂Te₃/organic thin film heterojunction photodetector with fast and wideband response from 450 to 3500 nanometers. *ACS Nano*. (2019) 13:755–63. doi: 10.1021/acsnano.8b08056
46. Yu YQ, Li Z, Lu ZJ, Geng XS, Lu YC, Xu GB, et al. Graphene/MoS₂/Si nanowires Schottky-NP Bipolar van der Waals heterojunction for ultrafast photodetectors. *IEEE Electron Device Lett*. (2018) 39:1688–91. doi: 10.1109/LED.2018.2872107
47. Tao L, Chen ZF, Li XM, Yan KY, Xu JB. Hybrid graphene tunneling photoconductor with interface engineering towards fast photoresponse and high responsivity. *npj 2D Mater Appl*. (2017) 1:32. doi: 10.1038/s41699-017-0028-0
48. Zhang Y, Yu YQ, Mi LF, Wang H, Zhu ZF, Wu QY, et al. *In situ* fabrication of vertical multilayered MoS₂/Si homotype heterojunction for high-speed visible-near-infrared photodetectors. *Small*. (2016) 12:1062–71. doi: 10.1002/smll.201502923

Conflict of Interest: The authors declare that the research was conducted in the absence of any commercial or financial relationships that could be construed as a potential conflict of interest.

Copyright © 2021 Liu, Yang, Zhang, Yang, Wang, Zheng and Gou. This is an open-access article distributed under the terms of the Creative Commons Attribution License (CC BY). The use, distribution or reproduction in other forums is permitted, provided the original author(s) and the copyright owner(s) are credited and that the original publication in this journal is cited, in accordance with accepted academic practice. No use, distribution or reproduction is permitted which does not comply with these terms.